

© 2022 Optical Society of America. Users may use, reuse, and build upon the article, or use the article for text or data mining, so long as such uses are for non-commercial purposes and appropriate attribution is maintained. All other rights are reserved—the terms of their open access agreement apply to all OSA formatted accepted versions of journal articles.

<https://doi.org/10.1364/OL.448477>

Access to this work was provided by the University of Maryland, Baltimore County (UMBC) ScholarWorks@UMBC digital repository on the Maryland Shared Open Access (MD-SOAR) platform.

Please provide feedback

Please support the ScholarWorks@UMBC repository by emailing scholarworks-group@umbc.edu and telling us what having access to this work means to you and why it's important to you. Thank you.

The Continuous Spectrum of Periodically Stationary Pulses in a Stretched Pulse Laser

VRUSHALY SHINGLOT^{1,*}, JOHN ZWECK¹, AND CURTIS MENYUK²

¹Department of Mathematical Sciences, The University of Texas at Dallas, Richardson, TX 75080, USA

²Department of Computer Science and Electrical Engineering, The University of Maryland Baltimore County, Baltimore, MD 21250, USA

*vks160330@utdallas.edu

Compiled January 18, 2022

A spectral method for determining the stability of periodically stationary pulses in fiber lasers is introduced. Pulse stability is characterized in terms of the spectrum (eigenvalues) of the monodromy operator, which is the linearization of the round trip operator about a periodically stationary pulse. A formula for the continuous (essential) spectrum of the monodromy operator is presented, which quantifies the growth and decay of continuous waves far from the pulse. The formula is verified by comparison with a fully numeric method for an experimental fiber laser. Finally, the effect of the saturable absorber on pulse stability is demonstrated. ©

2022 Optica Publishing Group

<http://dx.doi.org/10.1364/ao.XX.XXXXXX>

1. INTRODUCTION

Since the advent of the soliton laser, researchers have invented several generations of short pulse fiber lasers for a variety of applications, including stretched-pulse (dispersion-managed) lasers [1, 2], similariton lasers [3, 4], and the Mamyshev oscillator [5–7]. A significant modeling challenge is that from one generation to the next there has been a dramatic increase in the amount by which the pulse varies over each round trip. As is highlighted in the survey paper of Turitsyn et al. [8], the computational modeling of modern short pulse lasers should therefore be based on lumped models in which the pulse changes shape as it propagates through the various components of the laser system, returning to the same shape once per round trip. We call such pulses periodically stationary pulses to distinguish them from the stationary pulses in a soliton laser.

A key design issue is to determine those regions in parameter space in which the laser operates stably, and within that space to optimize the pulse parameters. In [8, 9], the authors develop a lumped laser model based on the Haus master equation with dispersion management and discrete dissipative elements. Using a chirped Gaussian pulse ansatz, they derive a reduced system of ordinary differential equations for the peak power, pulse width, and chirp, which they solve numerically to obtain periodically stationary pulses. This reduced method enables rapid exploration of the parameter space of the laser system.

Menyuk and Wang [10] describe the evolutionary and dynamical

approaches for determining pulse stability. In the evolutionary approach, an initial pulse is propagated many round trips of the laser. If the pulse converges to a stationary or periodically stationary pulse it is deemed to be stable. For the application of the dynamical approach to stationary solutions of averaged models [10–12], a numerical root finding method is first used to discover a stationary pulse. The stability of this pulse is then determined by computing the spectrum (set of eigenvalues) of the linearization of the differential equation about the pulse.

Cuevas-Maraver et al. [13] used the dynamical approach to determine the stability of the Kuznetsov-Ma breather, which is a periodically stationary analytical solution of the nonlinear Schrödinger equation. By approximating the nonlinear Schrödinger equation as a system of ordinary differential equations, Floquet theory [14] can be used to assess the stability of a periodic solution, ψ , in terms of the spectrum of the monodromy matrix. The monodromy matrix is the matrix, \mathbf{M} , for which the solution after one period of the linearization of the differential equation is obtained by multiplying an initial vector, \mathbf{u}_0 , by \mathbf{M} . Eigenvectors of \mathbf{M} whose eigenvalues lie outside the unit circle in the complex plane correspond to perturbations of ψ that grow from one period to the next. Tsoy et al. [15] found periodically stationary solutions of the cubic-quintic complex Ginzburg-Landau equation, which is an averaged model for pulse propagation in a fiber laser. Recently, Zweck et al. [16] derived a formula for the continuous (or essential) spectrum of the monodromy operator for these pulses. The continuous spectrum, which typically consists of a pair of continuous curves in the complex plane, quantifies the growth or decay of perturbations seeded by continuous waves far from the pulse, in contrast to the discrete spectrum that quantifies the growth and decay of perturbations that distort the modelocked pulse.

As the number of points used to discretize the pulse and the width of the time window both increase, the set of eigenvalues of the monodromy matrix converges to the spectrum of the monodromy operator. However, the rate of convergence is often very poor [11], particularly for the continuous spectrum since very large time windows are needed due to the slow decay of the corresponding eigenfunctions. However, since the pulse only affects the continuous spectrum through its contribution to the gain and loss via slow saturation, the continuous spectrum is relatively easy to compute, particularly for stationary pulses [11].

Although the dynamical approach has been extensively applied to stationary pulse solutions of averaged equations [10–

[12, 17–19], the results in this paper are the first application of the dynamical approach to periodically stationary pulse solutions of a lumped laser model. In particular, we build upon the results of Zweck et al. [16] by deriving a formula for the continuous spectrum of the monodromy operator of a periodically stationary pulse in a lumped model of a fiber laser. Because the full spectrum consists of the continuous spectrum together with only a few discrete eigenvalues, this result is a significant step towards determining the stability of periodically stationary pulses. The main advantage of our approach compared to that of Turitsyn et al [8, 9] is that changes in the spectrum of the monodromy operator provide insight into the physical mechanisms by which the pulse becomes unstable. Furthermore, as in soliton perturbation theory [20] and in the analysis of wake modes in SESAM fiber lasers [18], we anticipate that the eigenfunctions of the monodromy operator could be used to quantify the effects of noise without the need for Monte Carlo simulations.

2. FIBER LASER MODEL

We consider a lumped model of a fiber laser that is based on a stretched pulse laser of Kim et al. [2]. Although our results are formulated for this specific laser, the formula we present below for the continuous spectrum can be readily adapted to a wide range of short pulse fiber lasers. As we see in the system diagram in Fig. 1, the components in the lumped model are a saturable absorber (SA), two segments of single mode fiber (SMF1 and SMF2), a fiber amplifier (FA), a dispersion compensation element (DCF), and an output coupler (OC), arranged in a loop.

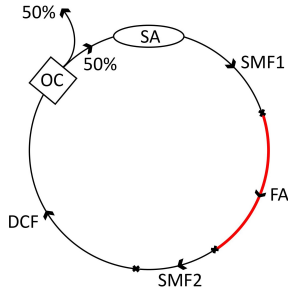


Fig. 1. System diagram of the stretched pulse laser described in [2] that we use for the results in sections 3 and 4.

We let $\psi = \psi(z, t)$ denote the complex electric field envelope of the pulse at position, z , in the loop and at retarded time, t , across the pulse. We let \mathcal{P} denote the transfer function of a component, so that $\psi_{\text{out}} = \mathcal{P}\psi_{\text{in}}$, where ψ_{in} and ψ_{out} are the pulses entering and leaving the component. The round trip operator,

$$\mathcal{R} = \mathcal{P}^{\text{OC}} \circ \mathcal{P}^{\text{DCF}} \circ \mathcal{P}^{\text{SMF2}} \circ \mathcal{P}^{\text{FA}} \circ \mathcal{P}^{\text{SMF1}} \circ \mathcal{P}^{\text{SA}}, \quad (1)$$

is the composition of the transfer functions of all the components.

We model the transfer function, \mathcal{P}^{FA} , of a fiber amplifier of length, L_{FA} , as $\psi_{\text{out}} = \mathcal{P}^{\text{FA}}\psi_{\text{in}}$, where $\psi_{\text{out}} = \psi(L_{\text{FA}}, t)$ is obtained by solving the initial value problem

$$\partial_z \psi = \left[\frac{g(z)}{2} \left(1 + \frac{1}{\Omega_g^2} \partial_t^2 \right) - \frac{i}{2} \beta \partial_t^2 + i\gamma |\psi|^2 \right] \psi, \quad (2)$$

$$\psi(0, t) = \psi_{\text{in}}(t).$$

Here, $g(z)$ is the saturable gain given by

$$g(\psi) = \frac{g_0}{1 + E(z)/E_{\text{sat}}}, \quad (3)$$

where, g_0 is the unsaturated gain, $E(z)$ is the pulse energy at position, z , and E_{sat} is the saturation energy. The finite bandwidth of the amplifier is modeled using a Gaussian filter with bandwidth, Ω_g . We model the transfer function, \mathcal{P}^{SMF} , of a segment of single mode fiber of length L_{SMF} by substituting $g_0 = 0$ in Eq. (3). Similarly, \mathcal{P}^{DCF} , is obtained by setting g_0 and $\gamma = 0$.

We model the saturable absorber using the fast saturable loss transfer function [17], \mathcal{P}^{SA} , given by

$$\psi_{\text{out}} = \mathcal{P}^{\text{SA}}(\psi_{\text{in}}) = \left(1 - \frac{\ell_0}{1 + |\psi_{\text{in}}|^2/P_{\text{sat}}} \right) \psi_{\text{in}}, \quad (4)$$

where ℓ_0 is the unsaturated loss and P_{sat} is the saturation power. With this model, ψ_{out} at time t only depends on ψ_{in} at the same time, t . Finally, we model the transfer function, \mathcal{P}^{OC} , of the output coupler as

$$\psi_{\text{out}} = \mathcal{P}^{\text{OC}}\psi_{\text{in}} = \sqrt{L_{\text{OC}}}\psi_{\text{in}}, \quad (5)$$

where L_{OC} is the power loss at the output coupler.

We choose the parameters for the model to be similar to those in the experimental stretched pulse laser of Kim [2]. The parameters for the saturable absorber are given in section 4. The saturable absorber is followed by a segment of single mode fiber with $\gamma = 2 \times 10^{-3} \text{ (Wm)}^{-1}$, $\beta = 10 \text{ kfs}^2/\text{m}$, and $L = 0.32 \text{ m}$, a fiber amplifier with $g_0 = 6\text{m}^{-1}$, $E_{\text{sat}} = 200 \text{ pJ}$, $\Omega_g = 50 \text{ THz}$, $\gamma = 4.4 \times 10^{-3} \text{ (Wm)}^{-1}$, $\beta = 25 \text{ kfs}^2/\text{m}$, and $L = 0.22 \text{ m}$, a second segment of SMF with $L = 0.11 \text{ m}$, a dispersion compensation element with $\beta = -1 \text{ kfs}^2$, and a 50% output coupler.

A periodically stationary pulse is a pulse, $\psi^{(0)}$, for which

$$\mathcal{R}\psi^{(0)} = e^{i\theta}\psi^{(0)}, \quad (6)$$

for some constant phase, θ . We formulate the problem of discovering a periodically stationary pulse as that of finding a zero of the residual,

$$\mathcal{E}(\psi^{(0)}, \theta) = \frac{1}{2} \int_{-\infty}^{\infty} |\mathcal{R}\psi^{(0)}(t) - e^{i\theta}\psi^{(0)}(t)|^2 dt. \quad (7)$$

Since $\mathcal{E} \geq 0$, in practice we minimize \mathcal{E} with respect to $\psi^{(0)}$ and θ using a gradient-based iterative optimization method.

To assess the stability of a periodically stationary pulse, ψ , in the presence of perturbations, we linearize the round trip operator, \mathcal{R} , about ψ . Because the linearization of Eq. (2) involves the complex conjugate of ψ , we reformulate the equations in the model as a system of equations for a real column vector $\boldsymbol{\psi} = [\Re(\psi), \Im(\psi)]^T = [\psi_1, \psi_2]^T$. We linearize the transfer function of each component using a perturbation $\boldsymbol{\psi}_\epsilon = \boldsymbol{\psi} + \epsilon \mathbf{u}$ about $\boldsymbol{\psi}$. For example, for a single mode fiber segment, the linearized transfer function is given by $\mathbf{u}_{\text{out}} = \mathcal{U}^{\text{SMF}} \mathbf{u}_{\text{in}}$, where $\mathbf{u}_{\text{out}} = \mathbf{u}(L_{\text{SMF}}, t)$ is obtained by solving the linearized initial value problem¹

$$\partial_z \mathbf{u} = (\mathbf{L} + \mathbf{M}_1(\boldsymbol{\psi}) + \mathbf{M}_2(\boldsymbol{\psi})) \mathbf{u}, \quad (8)$$

$$\mathbf{u}(0, t) = \mathbf{u}_{\text{in}},$$

where

$$\mathbf{L} = -\frac{\beta}{2} \mathbf{J} \partial_t^2, \quad \mathbf{M}_1(\boldsymbol{\psi}) = \gamma(\psi_1^2 + \psi_2^2) \mathbf{J}, \quad \mathbf{M}_2(\boldsymbol{\psi}) = 2\gamma \mathbf{J} \boldsymbol{\psi} \boldsymbol{\psi}^T,$$

¹See Supplement 1 for the derivation of this equation, and for formulae for the linearizations of the other transfer functions in the model.

with $\mathbf{J} = \begin{bmatrix} 0 & -1 \\ 1 & 0 \end{bmatrix}$. The linearization of the round trip operator, \mathcal{R} , about ψ determines whether or not a perturbation, \mathbf{u} , grows from round trip to round trip. This linear operator, which is called the monodromy operator for ψ , is given by

$$\mathcal{M} = \mathcal{U}^{\text{OC}} \circ \mathcal{U}^{\text{DCF}} \circ \mathcal{U}^{\text{SMF2}} \circ \mathcal{U}^{\text{FA}} \circ \mathcal{U}^{\text{SMF1}} \circ \mathcal{U}^{\text{SA}}, \quad (9)$$

where each operator \mathcal{U} is the linearization of the corresponding transfer function \mathcal{P} about ψ . A fundamental result of the Floquet theory of periodic differential equations asserts that a periodic pulse is stable if the spectrum of \mathcal{M} lies on or inside the unit disc in the complex plane, and that ψ is unstable if at least one eigenvalue of \mathcal{M} lies outside the unit disc [14].

3. FORMULA FOR THE CONTINUOUS SPECTRUM

The spectrum of a linear operator, \mathcal{M} , on a function space consists of the set of eigenvalues together with the continuous (essential) spectrum, $\sigma_{\text{cont}}(\mathcal{M})$. Since the continuous spectrum quantifies the growth rate of continuous waves far from the pulse, it is given in terms of the asymptotic monodromy operator,

$$\mathcal{M}_{\infty} = \mathcal{U}_{\infty}^{\text{OC}} \circ \mathcal{U}_{\infty}^{\text{DCF}} \circ \mathcal{U}_{\infty}^{\text{SMF2}} \circ \mathcal{U}_{\infty}^{\text{FA}} \circ \mathcal{U}_{\infty}^{\text{SMF1}} \circ \mathcal{U}_{\infty}^{\text{SA}}, \quad (10)$$

where, for each component, \mathcal{U}_{∞} is obtained by setting $\psi = 0$ in the corresponding operator \mathcal{U} .

The continuous spectrum of \mathcal{M}_{∞} consists of all complex λ for which there is a real μ and a nonzero $\mathbf{w} \in \mathbb{C}^2$ so that $\mathcal{M}_{\infty} e^{i\mu t} \mathbf{w} = \lambda e^{i\mu t} \mathbf{w}$. For the lumped model of the laser shown in Fig. 1, the set of all such $\lambda = \lambda(\mu)$ consists of the complex conjugate pair of curves parameterized by

$$\lambda_{\pm}(\mu) = \frac{1}{\sqrt{2}}(1 - \ell_0) \times \exp \left\{ \frac{1}{2} \left(1 - \frac{\mu^2}{\Omega_g^2} \right) \int_0^{L_{\text{FA}}} g(z) dz \right\} \exp \left\{ \pm i \frac{\mu^2}{2} \beta_{\text{RT}} \right\}, \quad (11)$$

for all $\mu \in \mathbb{R}$. Here β_{RT} is the round trip dispersion. In this case, the continuous spectrum consists of a pair of counter-rotating spirals whose amplitudes decay to zero as fast as a Gaussian decays to zero as $\mu \rightarrow \pm\infty$.

To ensure that a continuous wave with frequency μ experiences more loss than gain far from the pulse, we require that $|\lambda_{\pm}(\mu)| \leq 1$, which holds for all μ provided that

$$\frac{1}{2}(1 - \ell_0)^2 G_{\text{Tot}}^{\text{FA}} \leq 1, \quad (12)$$

where

$$G_{\text{Tot}}^{\text{FA}} = \exp \left\{ \int_0^{L_{\text{FA}}} g(z) dz \right\}. \quad (13)$$

If the root mean square width of the power spectral density of the pulse is sufficiently smaller than the gain bandwidth, then $G_{\text{Tot}}^{\text{FA}} \approx E_{\text{out}}^{\text{FA}} / E_{\text{in}}^{\text{FA}}$ is approximately the energy gain in the fiber amplifier. Eq. (12) is a necessary condition for stability since it ensures that continuous waves do not grow. Slow saturable gain plays a critical role in determining pulse stability since the gain experienced by the continuous waves decreases when the pulse energy increases. We note that because the loss saturates at high power, the gain and loss can still balance for the pulse. Consequently, the saturable absorber also plays a critical role in stabilizing the system [17]. While Eq. (11) is specific to the

model considered here, the basic approach of taking into account the impact of the pulse on the gain and loss experienced by continuous waves can be readily adapted to any ultrafast laser.

For an idealized soliton laser, continuous waves do not grow since the continuous spectrum lies entirely on the imaginary axis, rather than extending into the right half of the complex plane [20]. For periodically stationary solutions of the constant coefficient Ginzburg-Landau equation [16], the continuous spectrum lies in the open unit disc provided that the loss parameter of the equation is positive (i.e., linear loss exceeds linear gain). In both cases, the stability of continuous waves is independent of all other system parameters. However, for periodically stationary solutions in a fiber laser that includes a fiber amplifier with bandlimited gain saturation, the continuous spectrum, can depend in a complex way on the interplay between all the system parameters, since they all influence the shape of the pulse and hence the total gain, $G_{\text{Tot}}^{\text{FA}}$, in the fiber amplifier.

4. NUMERICAL RESULTS

In this section, we use Eq. (11) to calculate the continuous spectrum of the monodromy operator for periodically stationary pulses in a lumped model of an experimental femtosecond fiber laser. In particular, we demonstrate the effect that the parameters in the fast saturable absorber have on the continuous spectrum.

To compute periodically stationary pulses, we use an N -point discretization of the time window, which yields a discretized pulse $\psi = (\Re(\psi), \Im(\psi))$ in a $2N$ -dimensional Euclidean space, \mathbb{R}^{2N} . We then optimize the residual \mathcal{E} , which is a real-valued function on \mathbb{R}^{2N+1} , using the Broyden-Fletcher-Goldfarb-Shanno (BFGS) optimization algorithm [21]. To calculate the gradient of \mathcal{E} we adapted a method of Ambrose and Wilkening [22]. With this method, the cost of computing a directional derivative of \mathcal{E} is comparable to that of propagating a pulse and its linearization for one round trip through the laser. To obtain an initial guess for the optimization method we propagate a Gaussian pulse for a few round trips. Then we use optimization to drive the residual, \mathcal{E} , very close to zero, thereby obtaining a periodically stationary pulse. Once we have obtained a periodically stationary pulse, we verify Eq. (11) by computing the eigenvalues of the $2N \times 2N$ matrix discretization, \mathbf{M} , of the monodromy operator, \mathcal{M} . The computation of each column of \mathbf{M} involves solving an initial value problem for the linearized system for one round trip through the laser [13].

We consider two sets of parameters for the saturable absorber in the lumped model described in section 2. For parameter set 1, we choose $\ell_0 = 0.1$ and $P_{\text{sat}} = 2000$ W (weak saturation) and for parameter set 2, $\ell_0 = 0.2$ and $P_{\text{sat}} = 50$ W (strong saturation). In the far left panel of Fig. 2 we show the amplitude of the periodically stationary pulse at the output coupler as computed using the evolutionary method (solid blue) and the optimization method (dashed red). We observe that the wings on the sides of the solid blue pulse grow as the number of round trips increases in the evolutionary method, which suggests that the pulse may be unstable. In the center left panel, we show the set of all eigenvalues of the discretized monodromy matrix, \mathbf{M} , (blue circles) and the continuous spectrum, $\sigma_{\text{cont}}(\mathcal{M})$, obtained using Eq. (11) (solid red), both computed for the optimized pulse in the far left panel. The excellent agreement between the red and blue counter-rotating spirals provides a strong verification of Eq. (11). For this laser, the continuous spectrum of the monodromy operator is well approximated by a set of eigenvalues of \mathbf{M} , which coalesce to the continuous spectrum of \mathcal{M} as N increases. The spectral method shows that the periodically stationary pulse

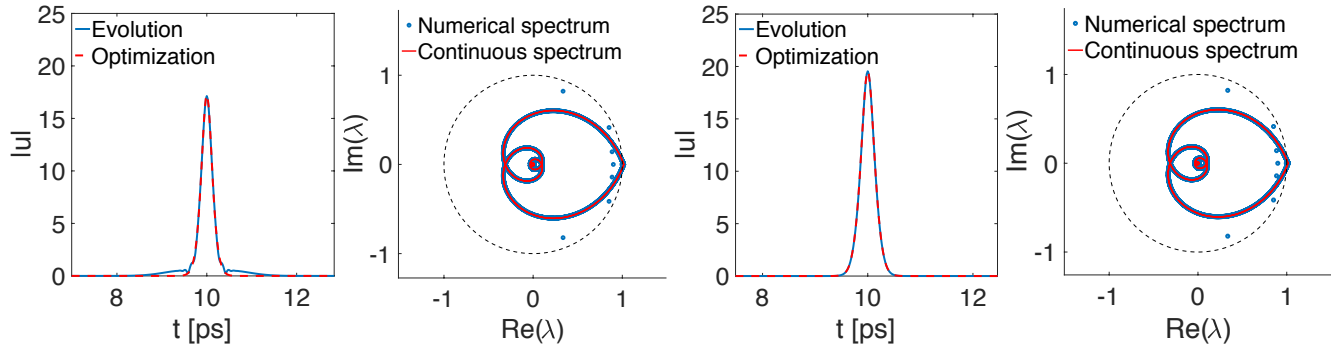


Fig. 2. Far left: Periodically stationary pulse obtained using the evolutionary approach (solid blue) and optimization (dashed red) for parameter set 1. Center left: Eigenvalues of the discretized monodromy matrix, \mathbf{M} , (blue circles) and the continuous spectrum, $\sigma_{\text{cont}}(\mathcal{M})$, computed using Eq. (11) (solid red). Center and far right: Corresponding results for parameter set 2.

is unstable, since $\sigma_{\text{cont}}(\mathcal{M})$ extends outside the unit circle near $\lambda = 1$. The largest eigenvalue on the real axis is at $\lambda = 1.0151$ using Eq. (11) and at $\lambda = 1.015$ using the numerical computation of the eigenvalues of \mathbf{M} . Indeed, if we evolve the optimized pulse for many round trips, low-frequency perturbations grow, generating a rising floor. These perturbations correspond to the small portion of the continuous spectrum that lies outside the unit circle. Physically, this result is to be expected since P_{sat} is much larger than the peak power of the pulse.

In the center and far right panels we show the corresponding results for parameter set 2. In this case, the pulse obtained using the evolutionary approach (solid blue), agrees very well with the optimized pulse (dashed red). More significantly, the spectrum of the optimized pulse lies inside the unit circle, which shows that this pulse is indeed stable. In this case, the largest eigenvalue on the real axis is at $\lambda = 0.8554$ using Eq. (11) and at $\lambda = 0.85538$ using the numerical method. We confirmed this conclusion by propagating the optimized pulse for many round trips. By increasing the unsaturated loss, ℓ_0 , in the saturable absorber so that Eq. (12) holds for parameter set 2, we have ensured that the growth of continuous waves is suppressed. Furthermore, by decreasing the saturation power, P_{sat} , to a value that is comparable to the pulse power, the pulse experiences less loss than does the continuum. As a consequence, the saturable gain effect in the fiber amplifier enables the system to balance the gain and loss of the pulse, which results in a pulse that is periodically stationary.²

Already in the 1975, Haus [23] identified the need for a saturable absorber to suppress the growth of continuous waves, while balancing gain and loss for the pulse. The importance of our work is to introduce a method that enables modelers to accurately quantify these effects in lasers for which there is significant pulse breathing. This full model approach complements previous reduced model approaches [8, 9] for determining regions in parameter space that support periodically stationary pulses. By computing the spectrum of the monodromy operator, we can rigorously assess the linear stability of periodically stationary pulses, identify the physical mechanisms that lead to instability, and ultimately quantify the effects of noise [10, 19].

Acknowledgment. JZ acknowledges support from the NSF under DMS-2106203. CRM acknowledges support from the NSF under ECCS-1807272.

Disclosure. The authors declare no conflicts of interest.

Supplemental document. See Supplement 1 for supporting content.

²See Supplement 1 for additional simulation results.

REFERENCES

1. K. Tamura, E. P. Ippen, H. A. Haus, and L. E. Nelson, *Opt. Lett.* **18**, 1080 (1993).
2. H. Kim, P. Qin, Y. Song, H. Yang, J. Shin, C. Kim, K. Jung, C. Wang, and J. Kim, *IEEE J. Sel. Top. Quantum Electron.* **20**, 260 (2014).
3. M. E. Fermann, V. I. Kruglov, B. C. Thomsen, J. M. Dudley, and J. D. Harvey, *Phys. Rev. Lett.* **84**, 6010 (2000).
4. I. Hartl, T. R. Schibli, A. Marcinkevicius, D. C. Yost, D. D. Hudson, M. E. Fermann, and J. Ye, *Opt. Lett.* **32**, 2870 (2007).
5. M. Rochette, L. R. Chen, K. Sun, and J. Hernandez-Cordero, *IEEE Photonics Technol. Lett.* **20**, 1497 (2008).
6. N. Tarasov, A. M. Perego, D. V. Churkin, K. Staliunas, and S. K. Turitsyn, *Nat. Commun.* **7**, 1 (2016).
7. P. Sidorenko, W. Fu, L. G. Wright, M. Olivier, and F. W. Wise, *Opt. Express* **43**, 2672 (2018).
8. S. K. Turitsyn, B. G. Bale, and M. P. Fedoruk, *Phys. Reports* **521**, 135 (2012).
9. B. G. Bale, O. G. Okhitnikov, and S. K. Turitsyn, "Modeling and technologies of ultrafast fiber lasers," in *Fiber Lasers*, O. G. Okhitnikov, ed. (Wiley-VCH Verlag GmbH, 2012), pp. 135–175.
10. C. R. Menyuk and S. Wang, *Nanophotonics* **5**, 332 (2016).
11. S. Wang, A. Docherty, B. S. Marks, and C. R. Menyuk, *J. Opt. Soc. Am. B* **31**, 2914 (2014).
12. Y. Shen, J. Zweck, S. Wang, and C. R. Menyuk, *Stud. Appl. Math.* **137**, 238 (2016).
13. J. Cuevas-Maraver, P. G. Kevrekidis, D. J. Frantzeskakis, N. I. Karachalios, M. Haragus, and G. James, *Phys. Rev. E* **96**, 012202 (2017).
14. G. Teschl, *Ordinary differential equations and dynamical systems*, vol. 140 (American Mathematical Society, 2012).
15. E. Tsoy, A. Ankiewicz, and N. Akhmediev, *Phys. Rev. E* **73**, 036621 (2006).
16. J. Zweck, Y. Latushkin, J. Marzuola, and C. Jones, *J. Evol. Equ.* **21**, 3313 (2021).
17. S. Wang, B. S. Marks, and C. R. Menyuk, *Opt. Express* **24**, 20228 (2016).
18. S. Wang, S. Droste, L. C. Sinclair, I. Coddington, N. R. Newbury, T. F. Carruthers, and C. R. Menyuk, *Opt. Lett.* **42**, 2362 (2017).
19. S. Wang, T. F. Carruthers, and C. R. Menyuk, *J. Opt. Soc. Am. B* **35**, 2521 (2018).
20. D. Kaup, *Phys. Rev. A* **42**, 5689 (1990).
21. J. Nocedal and S. Wright, *Numerical optimization* (Springer Science & Business Media, 2006).
22. D. M. Ambrose and J. Wilkening, "Computing time-periodic solutions of nonlinear systems of partial differential equations," in *Hyperbolic Problems: Theory, Numerics and Applications (In 2 Volumes)*, (World Scientific, 2012), pp. 273–280.
23. H. A. Haus, *J. Appl. Phys.* **46**, 3049 (1975).

FULL REFERENCES

1. K. Tamura, E. P. Ippen, H. A. Haus, and L. E. Nelson, "77-fs pulse generation from a stretched-pulse mode-locked all-fiber ring laser," *Opt. Lett.* **18**, 1080–1082 (1993).
2. H. Kim, P. Qin, Y. Song, H. Yang, J. Shin, C. Kim, K. Jung, C. Wang, and J. Kim, "Sub-20-attosecond timing jitter mode-locked fiber lasers," *IEEE J. Sel. Top. Quantum Electron.* **20**, 260–267 (2014).
3. M. E. Fermann, V. I. Kruglov, B. C. Thomsen, J. M. Dudley, and J. D. Harvey, "Self-similar propagation and amplification of parabolic pulses in optical fibers," *Phys. Rev. Lett.* **84**, 6010–6013 (2000).
4. I. Hartl, T. R. Schibli, A. Marcinkevicius, D. C. Yost, D. D. Hudson, M. E. Fermann, and J. Ye, "Cavity-enhanced similariton Yb-fiber laser frequency comb: 3×10^{14} W/cm² peak intensity at 136 MHz," *Opt. Lett.* **32**, 2870–2872 (2007).
5. M. Rochette, L. R. Chen, K. Sun, and J. Hernandez-Cordero, "Multi-wavelength and tunable self-pulsating fiber cavity based on regenerative SPM spectral broadening and filtering," *IEEE Photonics Technol. Lett.* **20**, 1497–1499 (2008).
6. N. Tarasov, A. M. Perego, D. V. Churkin, K. Staliunas, and S. K. Turitsyn, "Mode-locking via dissipative Faraday instability," *Nat. Commun.* **7**, 1–5 (2016).
7. P. Sidorenko, W. Fu, L. G. Wright, M. Olivier, and F. W. Wise, "Self-seeded, multi-megawatt, Mamyshev oscillator," *Opt. Express* **43**, 2672–2675 (2018).
8. S. K. Turitsyn, B. G. Bale, and M. P. Fedoruk, "Dispersion-managed solitons in fibre systems and lasers," *Phys. Reports* **521**, 135–203 (2012).
9. B. G. Bale, O. G. Okhitnikov, and S. K. Turitsyn, "Modeling and technologies of ultrafast fiber lasers," in *Fiber Lasers*, O. G. Okhitnikov, ed. (Wiley-VCH Verlag GmbH, 2012), pp. 135–175.
10. C. R. Menyuk and S. Wang, "Spectral methods for determining the stability and noise performance of passively modelocked lasers," *Nanophotonics* **5**, 332–350 (2016).
11. S. Wang, A. Docherty, B. S. Marks, and C. R. Menyuk, "Boundary tracking algorithms for determining the stability of mode-locked pulses," *J. Opt. Soc. Am. B* **31**, 2914–2930 (2014).
12. Y. Shen, J. Zweck, S. Wang, and C. R. Menyuk, "Spectra of short pulse solutions of the cubic–quintic complex Ginzburg–Landau equation near zero dispersion," *Stud. Appl. Math.* **137**, 238–255 (2016).
13. J. Cuevas-Maraver, P. G. Kevrekidis, D. J. Frantzeskakis, N. I. Karachalios, M. Haragus, and G. James, "Floquet analysis of Kuznetsov–Ma breathers: A path towards spectral stability of rogue waves," *Phys. Rev. E* **96**, 012202 (2017).
14. G. Teschl, *Ordinary differential equations and dynamical systems*, vol. 140 (American Mathematical Society, 2012).
15. E. Tsoy, A. Ankiewicz, and N. Akhmediev, "Dynamical models for dissipative localized waves of the complex Ginzburg–Landau equation," *Phys. Rev. E* **73**, 036621 (2006).
16. J. Zweck, Y. Latushkin, J. Marzuola, and C. Jones, "The essential spectrum of periodically stationary solutions of the complex Ginzburg–Landau equation," *J. Evol. Equ.* **21**, 3313–3329 (2021).
17. S. Wang, B. S. Marks, and C. R. Menyuk, "Comparison of models of fast saturable absorption in passively modelocked lasers," *Opt. Express* **24**, 20228–20244 (2016).
18. S. Wang, S. Droste, L. C. Sinclair, I. Coddington, N. R. Newbury, T. F. Carruthers, and C. R. Menyuk, "Wake mode sidebands and instability in mode-locked lasers with slow saturable absorbers," *Opt. Lett.* **42**, 2362–2365 (2017).
19. S. Wang, T. F. Carruthers, and C. R. Menyuk, "Efficiently modeling the noise performance of short-pulse lasers with a computational implementation of dynamical methods," *J. Opt. Soc. Am. B* **35**, 2521–2531 (2018).
20. D. Kaup, "Perturbation theory for solitons in optical fibers," *Phys. Rev. A* **42**, 5689–5694 (1990).
21. J. Nocedal and S. Wright, *Numerical optimization* (Springer Science & Business Media, 2006).
22. D. M. Ambrose and J. Wilkening, "Computing time-periodic solutions of nonlinear systems of partial differential equations," in *Hyperbolic Problems: Theory, Numerics and Applications (In 2 Volumes)*, (World Scientific, 2012), pp. 273–280.
23. H. A. Haus, "Theory of mode locking with a fast saturable absorber," *J. Appl. Phys.* **46**, 3049–3058 (1975).

The Continuous Spectrum of Periodically Stationary Pulses in a Stretched Pulse Laser

In this document we provide supplementary material for "The Continuous Spectrum of Periodically Stationary Pulses in a Stretched Pulse Laser". We first demonstrate how the periodically stationary pulse breathes over one round trip in the laser. Then, we provide a derivation of linearization of the round trip operator, \mathcal{R} , about a pulse, ψ . Finally, we present some additional numerical results to support the theory developed in the paper.

1. BREATHING OF A PULSE OVER ONE ROUND TRIP

In Fig. S1, we show how the periodically stationary pulse breathes over one-round trip of the laser. These results were obtained using the parameter set with the stronger saturable absorber ($\ell_0 = 0.2$, $P_{\text{sat}} = 50$ W). We plot the amplitude of the pulse exiting each component of the laser. We observe that the pulse undergoes significant changes before returning to its original shape at the end of the round trip.

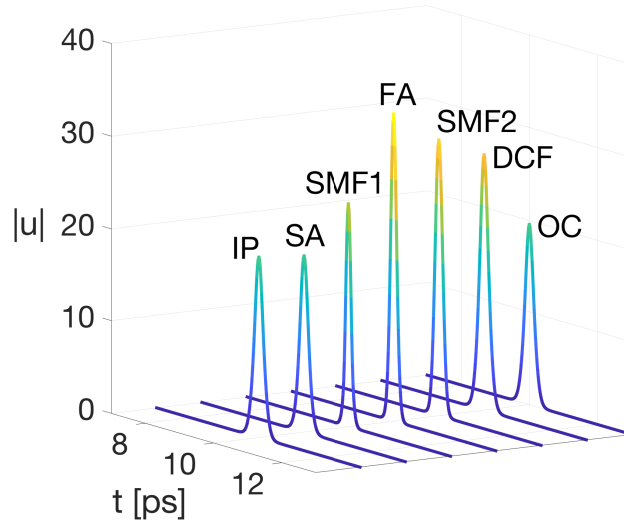


Fig. S1. Plot of the periodically stationary pulse associated with parameter set 2 showing the amplitude of the pulse exiting each component of the laser.

2. LINEARIZATION OF THE ROUND TRIP OPERATOR

As in Eq. (1) of the paper, we define the round trip operator, \mathcal{R} , to be the composition of the transfer functions of all the components of the laser given by

$$\mathcal{R} = \mathcal{P}^{\text{OC}} \circ \mathcal{P}^{\text{DCF}} \circ \mathcal{P}^{\text{SMF2}} \circ \mathcal{P}^{\text{FA}} \circ \mathcal{P}^{\text{SMF1}} \circ \mathcal{P}^{\text{SA}}. \quad (\text{S1})$$

Here, we regard each transfer function, \mathcal{P} , as acting on a column vector of the form $\psi = [\text{Re } \psi, \text{Im } \psi]^T = [\psi_1, \psi_2]^T$, where ψ is a complex valued function of t . By the chain rule, the linearization of \mathcal{R} about a pulse, ψ , is a composition of the linearizations, \mathcal{U} , of the individual transfer functions, \mathcal{P} . Therefore, the monodromy operator, \mathcal{M} , is given by

$$\mathcal{M} = \mathcal{U}^{\text{OC}} \circ \mathcal{U}^{\text{DCF}} \circ \mathcal{U}^{\text{SMF2}} \circ \mathcal{U}^{\text{FA}} \circ \mathcal{U}^{\text{SMF1}} \circ \mathcal{U}^{\text{SA}}. \quad (\text{S2})$$

Because eigenvalues and eigenvectors can be complex, we regard the transfer functions, \mathcal{U} , as acting on the column vectors of the form $u = [u_1, u_2]^T$, where each u_j is a complex valued function of t .

We first derive the linearized transfer function, \mathcal{U}^{FA} , corresponding to the transfer function, \mathcal{P}^{FA} , of the fiber amplifier about ψ . We rewrite the transfer function, \mathcal{P}^{FA} , of a fiber amplifier of length, L_{FA} , in terms of $\psi = (\psi_1, \psi_2)$ as

$$\psi_{\text{out}} = \mathcal{P}^{\text{FA}} \psi_{\text{in}}, \quad (\text{S3})$$

where $\boldsymbol{\psi}_{\text{out}}(t) = \boldsymbol{\psi}(\text{L}_{\text{FA}}, t)$ is obtained by solving the initial value problem

$$\begin{aligned}\partial_z \boldsymbol{\psi} &= \left[\frac{g(\boldsymbol{\psi})}{2} \left(1 + \frac{1}{\Omega_g^2} \partial_t^2 \right) - \frac{\beta}{2} \mathbf{J} \partial_t^2 + \gamma(\psi_1^2 + \psi_2^2) \mathbf{J} \right] \boldsymbol{\psi}, \\ \boldsymbol{\psi}(0, t) &= \boldsymbol{\psi}_{\text{in}}(t).\end{aligned}\tag{S4}$$

Here, $\mathbf{J} = \begin{bmatrix} 0 & -1 \\ 1 & 0 \end{bmatrix}$ and $g(\boldsymbol{\psi})$ is the saturable gain given by

$$g(\boldsymbol{\psi}) = \frac{g_0}{1 + \int_{-\infty}^{\infty} (\psi_1^2(t) + \psi_2^2(t)) dt / E_{\text{sat}}}.\tag{S5}$$

We use a perturbation, $\boldsymbol{\psi}_\epsilon = \boldsymbol{\psi} + \epsilon \mathbf{u}$, about $\boldsymbol{\psi}$ to linearize \mathcal{P}^{FA} . Throughout the following calculation, we ignore the terms of order ϵ^2 and higher. Using Eq. (S4) for both $\boldsymbol{\psi}$ and $\boldsymbol{\psi}_\epsilon$, we obtain

$$\begin{aligned}\partial_z \mathbf{u} &= \lim_{\epsilon \rightarrow 0} \frac{\partial_z \boldsymbol{\psi}_\epsilon - \partial_z \boldsymbol{\psi}}{\epsilon} \\ &= \lim_{\epsilon \rightarrow 0} \frac{1}{\epsilon} \left\{ \frac{g(\boldsymbol{\psi}_\epsilon)}{2} \left(1 + \frac{1}{\Omega_g^2} \partial_t^2 \right) \boldsymbol{\psi}_\epsilon - \frac{g(\boldsymbol{\psi})}{2} \left(1 + \frac{1}{\Omega_g^2} \partial_t^2 \right) \boldsymbol{\psi} \right\} \\ &\quad + \lim_{\epsilon \rightarrow 0} \frac{1}{\epsilon} \left\{ \left(-\frac{\beta}{2} \mathbf{J} \partial_t^2 + \gamma(\psi_{\epsilon,1}^2 + \psi_{\epsilon,2}^2) \mathbf{J} \right) \boldsymbol{\psi}_\epsilon - \left(-\frac{\beta}{2} \mathbf{J} \partial_t^2 + \gamma(\psi_1^2 + \psi_2^2) \mathbf{J} \right) \boldsymbol{\psi} \right\}.\end{aligned}\tag{S6}$$

To simplify the first term on right hand side of Eq. (S6), we observe that

$$g(\boldsymbol{\psi}_\epsilon) = g(\boldsymbol{\psi}) - \frac{2\epsilon g^2(\boldsymbol{\psi})}{g_0 E_{\text{sat}}} \int_{-\infty}^{\infty} \boldsymbol{\psi}^T(t) \mathbf{u}(t) dt.\tag{S7}$$

Therefore,

$$\begin{aligned}&\frac{g(\boldsymbol{\psi}_\epsilon)}{2} \left(1 + \frac{1}{\Omega_g^2} \partial_t^2 \right) \boldsymbol{\psi}_\epsilon - \frac{g(\boldsymbol{\psi})}{2} \left(1 + \frac{1}{\Omega_g^2} \partial_t^2 \right) \boldsymbol{\psi} \\ &= \frac{\epsilon g(\boldsymbol{\psi})}{2} \left(1 + \frac{1}{\Omega_g^2} \partial_t^2 \right) \mathbf{u} - \left(\frac{\epsilon g^2(\boldsymbol{\psi})}{g_0 E_{\text{sat}}} \int_{-\infty}^{\infty} \boldsymbol{\psi}^T u dt \right) \left(1 + \frac{1}{\Omega_g^2} \partial_t^2 \right) \boldsymbol{\psi}.\end{aligned}\tag{S8}$$

Simplifying the second term on the right hand side of Eq. (S6), we obtain

$$\begin{aligned}&\left(-\frac{\beta}{2} \mathbf{J} \partial_t^2 + \gamma(\psi_{\epsilon,1}^2 + \psi_{\epsilon,2}^2) \mathbf{J} \right) \boldsymbol{\psi}_\epsilon - \left(-\frac{\beta}{2} \mathbf{J} \partial_t^2 + \gamma(\psi_1^2 + \psi_2^2) \mathbf{J} \right) \boldsymbol{\psi} \\ &= -\frac{\epsilon \beta}{2} \mathbf{J} \partial_t^2 \mathbf{u} + \epsilon \gamma(\psi_1^2 + \psi_2^2) \mathbf{J} \mathbf{u} + 2\epsilon \gamma \mathbf{J} \boldsymbol{\psi} \boldsymbol{\psi}^T \mathbf{u}.\end{aligned}\tag{S9}$$

Substituting Eq. (S8) and Eq. (S9) in Eq. (S6), we find that the linearized transfer function, \mathcal{U}^{FA} , is given by

$$\mathbf{u}_{\text{out}} = \mathcal{U}^{\text{FA}} \mathbf{u}_{\text{in}},\tag{S10}$$

where $\mathbf{u}_{\text{out}} = \mathbf{u}(\text{L}_{\text{FA}}, t)$ is obtained by solving the linearized initial value problem

$$\begin{aligned}\partial_z \mathbf{u} &= (g(\boldsymbol{\psi}) \mathbf{K} + \mathbf{L} + \mathbf{M}_1(\boldsymbol{\psi}) + \mathbf{M}_2(\boldsymbol{\psi})) \mathbf{u} + \mathbf{P}(\boldsymbol{\psi})(\mathbf{u}), \\ \mathbf{u}(0, t) &= \mathbf{u}_{\text{in}},\end{aligned}\tag{S11}$$

where

$$\begin{aligned}\mathbf{K} &= \frac{1}{2} \left(1 + \frac{1}{\Omega_g^2} \frac{\partial^2}{\partial t^2} \right), \\ \mathbf{L} &= -\frac{\beta}{2} \mathbf{J} \partial_t^2, \\ \mathbf{M}_1(\boldsymbol{\psi}) &= \gamma(\psi_1^2 + \psi_2^2) \mathbf{J}, \\ \mathbf{M}_2(\boldsymbol{\psi}) &= 2\gamma \mathbf{J} \boldsymbol{\psi} \boldsymbol{\psi}^T,\end{aligned}\tag{S12}$$

and

$$\mathbf{P}(\boldsymbol{\psi})(\mathbf{u}) = -\frac{g^2(\boldsymbol{\psi})}{g_0 E_{\text{sat}}} \left(\left(1 + \frac{1}{\Omega_g^2} \frac{\partial^2}{\partial t^2} \right) \boldsymbol{\psi} \right) \int_{-\infty}^{\infty} \boldsymbol{\psi}^T(t) \mathbf{u}(t) dt\tag{S13}$$

is a nonlocal operator. When we discretize the time window, $[-T/2, T/2]$, the vector-valued functions, $\boldsymbol{\psi}$ and \mathbf{u} , are replaced by column vectors in the $2N$ -dimensional Euclidean space, \mathbb{R}^{2N} , which we also denote by $\boldsymbol{\psi}$ and \mathbf{u} . Then, the discretization of the nonlocal operator $\mathbf{P}(\boldsymbol{\psi})$ is given by the matrix-vector multiplication

$$\mathbf{P}(\boldsymbol{\psi}) \mathbf{u} = -\frac{g^2(\boldsymbol{\psi}) \Delta t}{g_0 E_{\text{sat}}} \left(\left(1 + \frac{1}{\Omega_g^2} \frac{\partial^2}{\partial t^2} \right) \boldsymbol{\psi} \right) \boldsymbol{\psi}^T \mathbf{u}.\tag{S14}$$

The linearized transfer function of a single mode fiber segment can be obtained by setting $g_0 = 0$ in the derivation above.

We now derive the linearized transfer function for the saturable absorber, \mathcal{U}^{SA} . The transfer function, \mathcal{P}^{SA} , of the saturable absorber is given by

$$\psi_{\text{out}} = \mathcal{P}^{\text{SA}}(\psi_{\text{in}}) = (1 - \ell(\psi_{\text{in}})) \psi_{\text{in}}, \quad (\text{S15})$$

where

$$\ell(\psi_{\text{in}}) = \frac{\ell_0}{1 + (\psi_{\text{in},1}^2 + \psi_{\text{in},2}^2)/P_{\text{sat}}}. \quad (\text{S16})$$

We use the perturbation $\psi_{\text{in},\epsilon} = \psi_{\text{in}} + \epsilon \mathbf{u}_{\text{in}}$ to linearize \mathcal{P}^{SA} about ψ_{in} . Here, $\psi_{\text{in},\epsilon}$ and ψ_{in} satisfy Eq. (S15). Therefore, we obtain

$$\begin{aligned} \mathbf{u}_{\text{out}} &= \lim_{\epsilon \rightarrow 0} \frac{\psi_{\text{in},\epsilon} - \psi_{\text{in}}}{\epsilon} \\ &= \lim_{\epsilon \rightarrow 0} \frac{1}{\epsilon} \left\{ (1 - \ell(\psi_{\text{in},\epsilon})) \psi_{\text{in},\epsilon} - (1 - \ell(\psi_{\text{in}})) \psi_{\text{in}} \right\} \\ &= \lim_{\epsilon \rightarrow 0} \left\{ \mathbf{u}_{\text{in}} - \ell(\psi_{\text{in},\epsilon}) \mathbf{u}_{\text{in}} - \frac{\ell(\psi_{\text{in},\epsilon}) - \ell(\psi_{\text{in}})}{\epsilon} \psi_{\text{in}} \right\}. \end{aligned} \quad (\text{S17})$$

Next, we use Eq. (S16) to obtain

$$\ell(\psi_{\text{in},\epsilon}) = \ell(\psi_{\text{in}}) - \frac{2\epsilon \ell^2(\psi_{\text{in}})}{\ell_0 P_{\text{sat}}} \psi_{\text{in}}^T \mathbf{u}_{\text{in}}. \quad (\text{S18})$$

Using Eq. (S18) in Eq. (S17), we finally obtain the linearized transfer function, \mathcal{U}^{SA} , given by

$$\mathbf{u}_{\text{out}} = \mathcal{U}^{\text{SA}}(\psi_{\text{in}})(\mathbf{u}_{\text{in}}) = \left(1 - \ell(\psi_{\text{in}}) - \frac{2\ell^2(\psi_{\text{in}})}{\ell_0 P_{\text{sat}}} \psi_{\text{in}} \psi_{\text{in}}^T \right) \mathbf{u}_{\text{in}}. \quad (\text{S19})$$

The remaining components, i.e. dispersion compensation fiber and output coupler, already have linear transfer functions.

3. ADDITIONAL NUMERICAL RESULTS

In the paper, we showed numerical results for two parameter sets, the first with a weaker saturable absorber ($\ell_0 = 0.1$, $P_{\text{sat}} = 2000$ W) and the second with a stronger saturable absorber ($\ell_0 = 0.2$, $P_{\text{sat}} = 50$ W). We chose these two parameter sets because with the first set the pulse is unstable and with the second set it is stable, and in both cases the stability of the pulse is determined by the essential spectrum rather than by the discrete eigenvalues. This is because for both parameter sets the largest magnitude of the points in the continuous spectrum always exceeds the magnitudes of the discrete eigenvalues. In this section, we present additional numerical results showing bifurcations from an unstable to a stable pulse by varying ℓ_0 and P_{sat} one at a time. First, we fix $\ell_0 = 0.05$ and decrease the value of P_{sat} from 1000 W to 200 W. Then, we fix $P_{\text{sat}} = 500$ W and increase ℓ_0 from 0.02 to 0.14. The other components of the laser have the same parameter values as given in Sec. 2 of the paper. From Eq. (6), we observe that as P_{sat} decreases, the loss near the center of the pulse increases, since the saturation absorption effect is stronger. Similarly, as ℓ_0 increases, the loss near the center of the pulse increases. For these parameter variations, as we vary P_{sat} or ℓ_0 , the stability of the pulse is determined by the continuous spectrum, since the largest magnitude of the points in the continuous spectrum always exceeds the magnitudes of the discrete eigenvalues.

In Fig. S2, we show results for $P_{\text{sat}} = 1000$ W (top row), $P_{\text{sat}} = 300$ W (middle row) and $P_{\text{sat}} = 200$ W (bottom row). In all three cases, we chose $\ell_0 = 0.05$. In the top left panel, we show the amplitude of the pulse at the output coupler as computed using the evolutionary method after 100 round trips (solid blue) and using the optimization method (dashed red). The small wings on the sides of the pulse computed using the evolutionary method suggest that this pulse is unstable. In the middle panel of the first row, we show the set of all eigenvalues of the discretized monodromy matrix, \mathbf{M} , (blue circles) and the continuous spectrum, $\sigma_{\text{cont}}(\mathcal{M})$, obtained using the formula given in the paper (solid red), both computed for the optimized pulse with $P_{\text{sat}} = 1000$ W. In the right panel, we show excellent agreement between the two spectra in a small neighbourhood of $\lambda = 1$. The largest eigenvalue on the real axis is $\lambda = 1.0146$ as obtained using the formula for the continuous spectrum and $\lambda = 1.0145$ as obtained using the numerical method. Therefore, the spectral method shows that the pulse is indeed unstable. To further verify this result, we propagated the perturbed pulse, $\psi_\epsilon = \psi + \epsilon \mathbf{u}$, through the system, where $\epsilon = 10^{-5}$ and \mathbf{u} is the normalized eigenvector corresponding to the eigenvalue with largest magnitude. In the top row of Fig. S3, we show the pulse, ψ_ϵ , after 4000 round trips, on a linear scale (left) and logarithmic scale (right), together with the optimized pulse. The relative L^2 error between these two pulses is 0.9837.

In the center rows of Fig. S2 and Fig. S3, we show the corresponding results for $P_{\text{sat}} = 300$ W. In this case, the wings on the sides of the pulse obtained with the evolutionary method (solid blue) are not as pronounced. The spectral method shows that the pulse is unstable since the largest eigenvalue on the real axis is $\lambda = 1.0013$ as obtained both using the

formula and with the numerical method. The relative L^2 error of between the evolved perturbed pulse, ψ_e , and the optimized pulse is 0.7494. In the left panel of Fig. S4, we plot the largest eigenvalue as a function of P_{sat} . We observe that this eigenvalue remains outside the unit circle as P_{sat} decreases from 1000 W and 300 W. Therefore, the pulse is unstable over this range of values of P_{sat} .

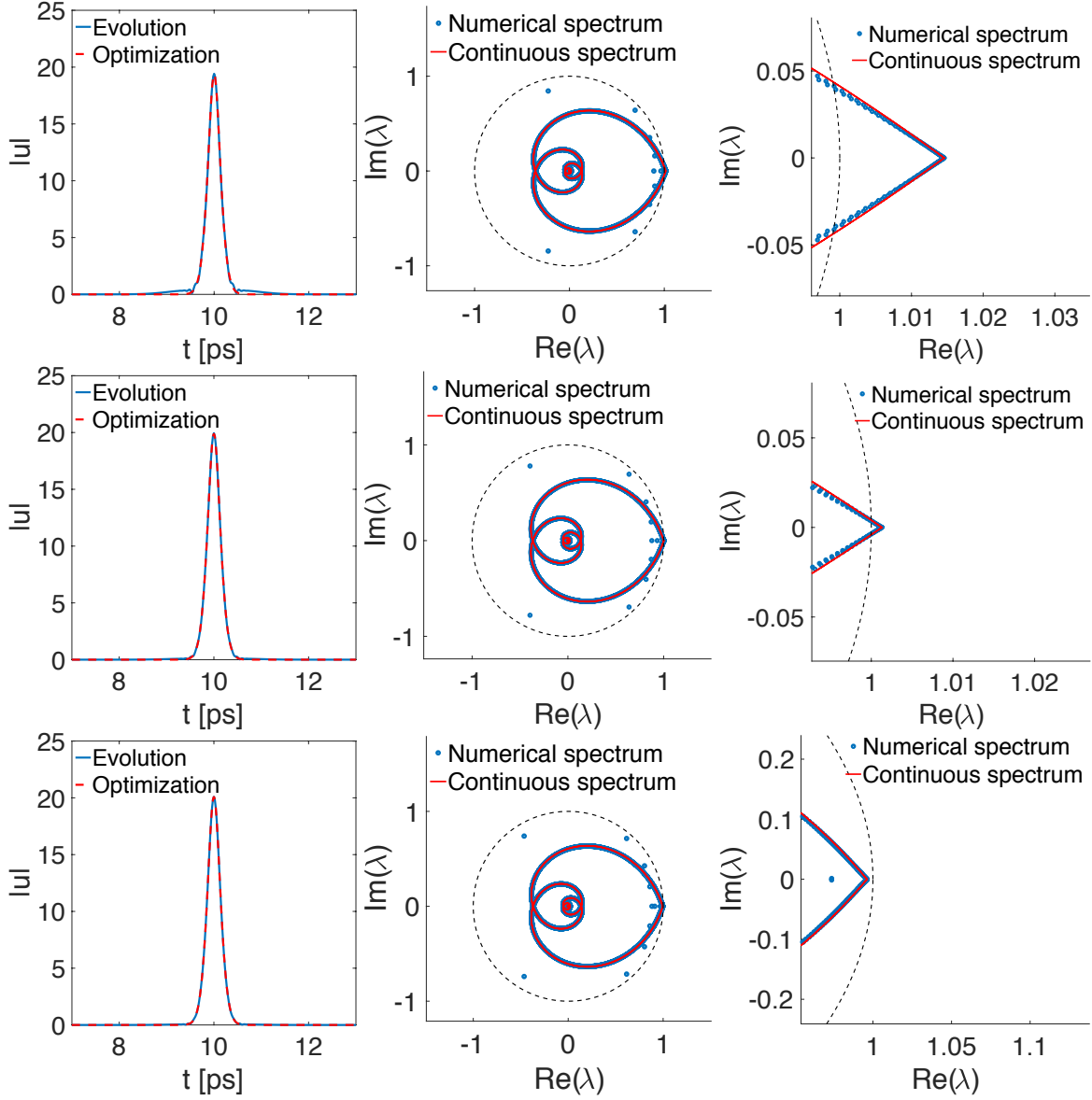


Fig. S2. Top row: Left: Periodically stationary pulses obtained using the evolutionary approach (solid blue) and optimization (dashed red) for $P_{\text{sat}} = 1000$ W. **Center and right:** Eigenvalues of the discretized monodromy matrix, \mathbf{M} , (blue circles) and the continuous spectrum, $\sigma_{\text{cont}}(\mathcal{M})$, computed using the formula given in paper (solid red) for optimized pulse. **Center and bottom rows:** Corresponding results for $P_{\text{sat}} = 300$ W and $P_{\text{sat}} = 200$ W, respectively. In all three cases, $\ell_0 = 0.05$.

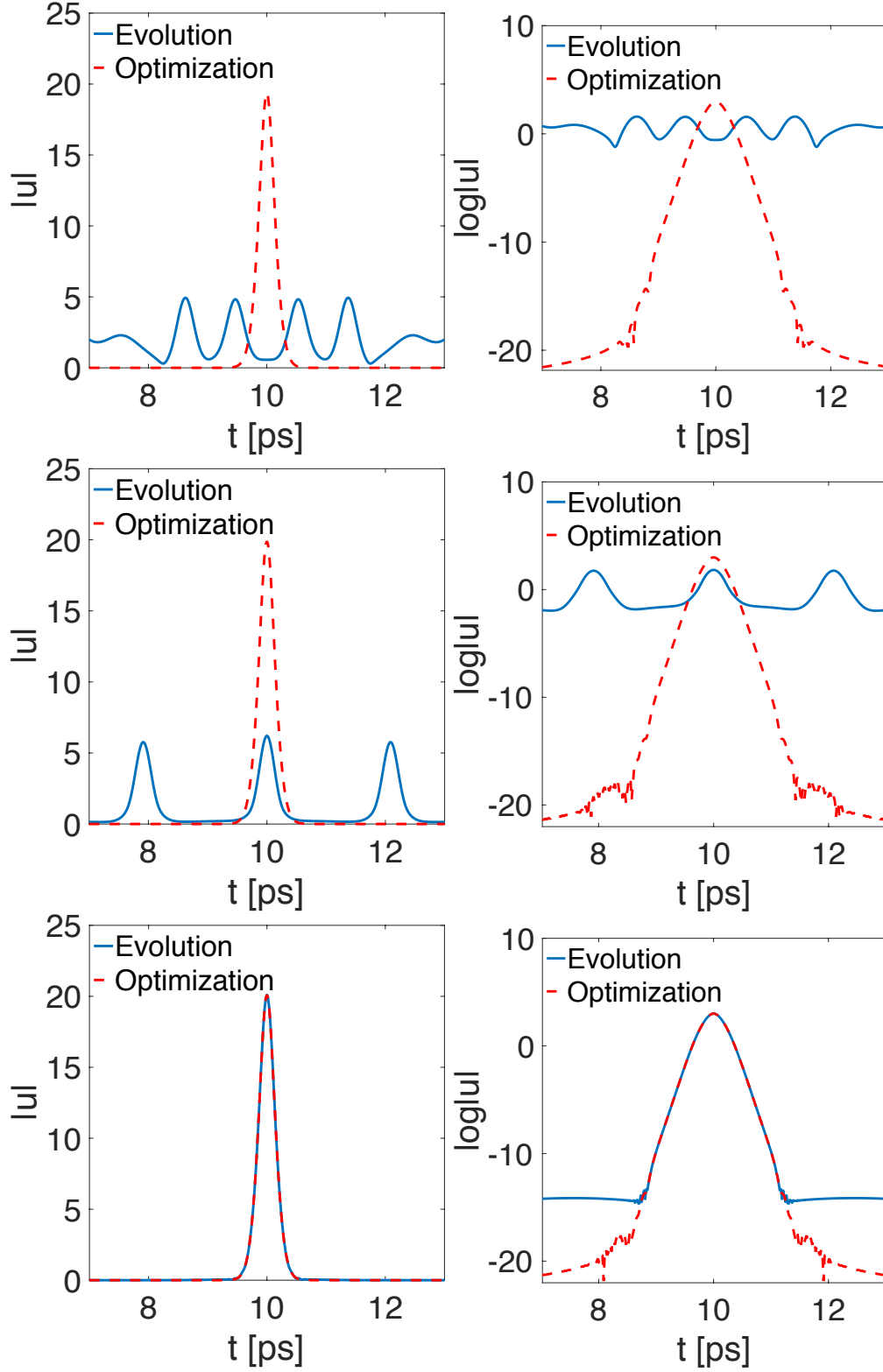


Fig. S3. **Top row:** Left: Perturbed optimized pulse, ψ_e , at the output coupler after evolution over 4000 round trips (solid blue) and the optimized pulse (dashed red) for $P_{\text{sat}} = 1000$ W. **Right:** Corresponding results on a log scale. **Center and bottom rows:** Corresponding results for $P_{\text{sat}} = 300$ W and $P_{\text{sat}} = 200$ W, respectively. In all three cases, $\ell_0 = 0.05$.

In the bottom rows of Fig. S2 and Fig. S3, we show the corresponding results for $P_{\text{sat}} = 200$ W. In this case, the periodically stationary pulse obtained using the evolutionary method agrees very well with the one obtained using the optimization method. Further, the spectrum of the optimized pulse lies inside the unit circle with the largest eigenvalue on the real axis $\lambda = 0.99618$ as obtained using the formula and $\lambda = 0.99616$ as obtained using the numerical method. Finally, the evolved perturbed pulse, ψ_ϵ , also agrees very well with the optimized pulse with the relative L^2 error 3.9005×10^{-4} . Therefore, using these observations we conclude that when $P_{\text{sat}} = 200$ the periodically stationary pulse is stable. In conclusion, these results show that as the saturation absorption effect becomes stronger, the pulse transitions from being unstable to being stable.

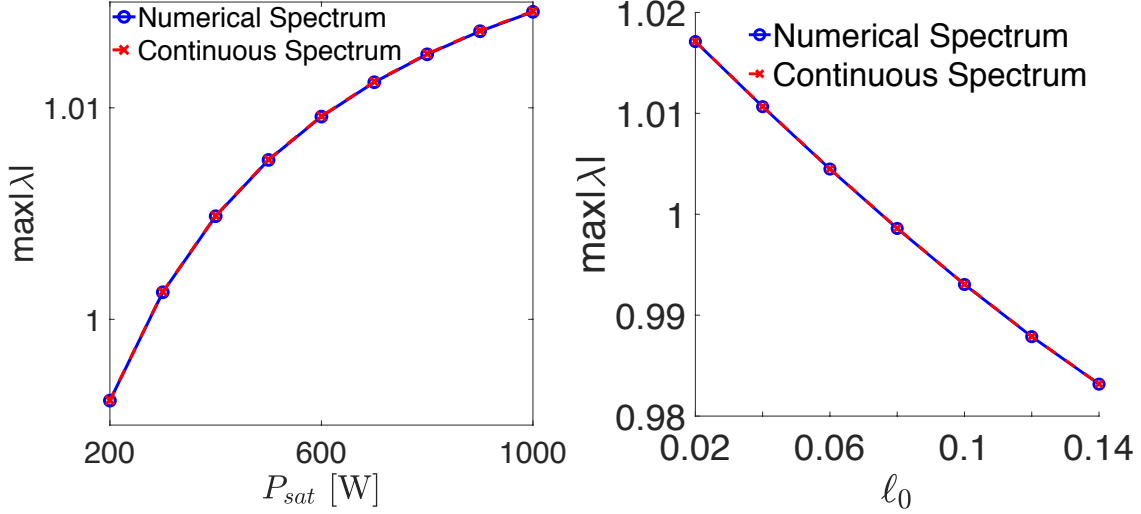


Fig. S4. Left: A plot of the maximum real eigenvalue, $\max|\lambda|$, vs. P_{sat} showing a bifurcation from a stable to an unstable pulse. Here, $\ell_0 = 0.05$. Right: Corresponding plot in which ℓ_0 is varied and $P_{\text{sat}} = 500$ W.

In Fig. S5, we present results similar to Fig. S2 for $\ell_0 = 0.02$ (top row), $\ell_0 = 0.06$ (middle row) and $\ell_0 = 0.08$ (bottom row). In all three cases, $P_{\text{sat}} = 500$ W. In the top left panel, the small wings on the sides of the pulse computed using the evolutionary method suggest that this pulse is unstable. The largest eigenvalue on the real axis is $\lambda = 1.0171$ as obtained using the formula for the continuous spectrum as well as using the numerical method. Therefore, the spectral method shows that the pulse is indeed unstable.

In the center rows of Fig. S5, we show the corresponding results for $\ell_0 = 0.06$. In this case, the wings on the sides of the pulse obtained with the evolutionary method (solid blue) are not as pronounced. The spectral method shows that the pulse is unstable since the largest eigenvalue on the real axis is $\lambda = 1.0045$ as obtained using both the methods. Since the maximum eigenvalue remains outside the unit circle as ℓ_0 increases from 0.02 to 0.06, the pulse is unstable over this range of values of ℓ_0 . This behavior is also shown in the right panel of Fig. S4, where we plot the largest eigenvalue as a function of ℓ_0 .

In the bottom rows of Fig. S5, we show the corresponding results for $\ell_0 = 0.08$. In this case, the periodically stationary pulse obtained using the evolutionary method agrees very well with the one obtained using the optimization method. Further, the spectrum of the optimized pulse lies inside the unit circle with the largest eigenvalue on the real axis $\lambda = 0.99862$ as obtained using the formula and $\lambda = 0.99859$ as obtained using the numerical method. Therefore, we conclude that the periodically stationary pulse associated with $\ell_0 = 0.08$ is stable. From the plot in the right panel of Fig. S4, we observe that the periodically stationary pulses remain stable as ℓ_0 increases from 0.08 to 0.14. In conclusion, these results show that as the saturation absorption effect becomes stronger, the pulse transitions from being unstable to being stable.

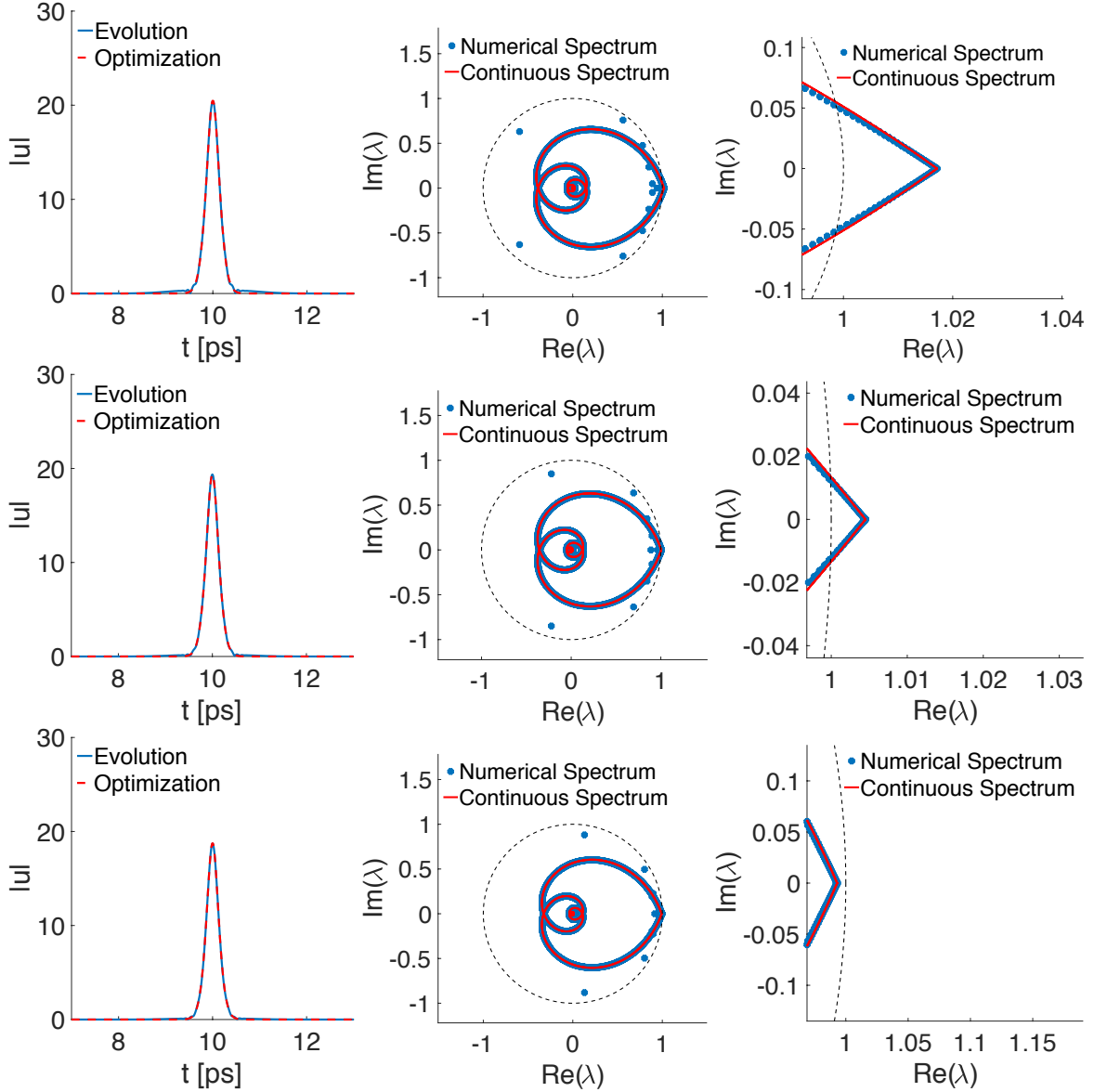


Fig. S5. Top row: Left: Periodically stationary pulses obtained using the evolutionary approach (solid blue) and optimization (dashed red) for $\ell_0 = 0.02$. Center and right: Eigenvalues of the discretized monodromy matrix, \mathbf{M} , (blue circles) and the continuous spectrum, $\sigma_{\text{cont}}(\mathcal{M})$, computed using the formula given in paper (solid red) for optimized pulse. Center and bottom rows: Corresponding results for $\ell_0 = 0.06$ and $\ell_0 = 0.08$, respectively. In all three cases, $P_{\text{sat}} = 500$ W.